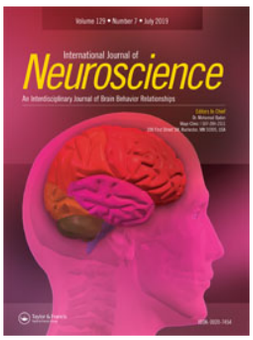

International Journal of Neuroscience

ISSN: 0020-7454 (Print) 1543-5245 (Online) Journal homepage: https://www.tandfonline.com/loi/ines20

Computational investigation of mechanistic insights of Aβ42 interactions against extracellular domain of nAChRα7 in Alzheimer's disease

Mubashir Hassan, Saba Shahzadi, Hussain Raza, Muhammad Athar Abbasi, Hany Alashwal, Nazar Zaki, Ahmed A. Moustafa & Sung-Yum Seo

To cite this article: Mubashir Hassan, Saba Shahzadi, Hussain Raza, Muhammad Athar Abbasi, Hany Alashwal, Nazar Zaki, Ahmed A. Moustafa & Sung-Yum Seo (2019) Computational investigation of mechanistic insights of Aβ42 interactions against extracellular domain of nAChRα7 in Alzheimer's disease, International Journal of Neuroscience, 129:7, 666-680, DOI: 10.1080/00207454.2018.1543670

To link to this article: https://doi.org/10.1080/00207454.2018.1543670

Accepted author version posted online: 13 Nov 2018.
Published online: 09 Jan 2019.

INTERNATIONAL JOURNAL OF NEUROSCIENCE
2019, VOL. 129, NO. 7, 666–680
https://doi.org/10.1080/00207454.2018.1543670

Taylor & Francis
Taylor & Francis Group

ORIGINAL ARTICLE

Computational investigation of mechanistic insights of Aβ42 interactions against extracellular domain of nAChRα7 in Alzheimer's disease

Mubashir Hassan[a], Saba Shahzadi[b,c], Hussain Raza[a], Muhammad Athar Abbasi[a,d], Hany Alashwal[e], Nazar Zaki[e], Ahmed A. Moustafa[f,g,h] and Sung-Yum Seo[a]

[a]Department of Biological Sciences, College of Natural Sciences, Kongju National University, Gongju, Chungnam-do 32588, Republic of Korea; [b]Institute of Molecular Science and Bioinformatics, Lahore, Pakistan; [c]Department of Bioinformatics, Virtual University of Pakistan, Lahore, Pakistan; [d]Department of Chemistry, Government College University, Lahore, Pakistan; [e]Department of Computer Science and Software Engineering, College of Information Technology, United Arab Emirates University, Al-Ain, United Arab Emirates; [f]School of Social Sciences and Psychology; [g]MARCS Institute for Brain and Behaviour, Western Sydney University, Sydney, New South Wales, Australia; [h]Department of Social Sciences, College of Arts and Sciences, Qatar University, Doha, Qatar'

ABSTRACT

Aim: Amyloid beta (Aβ) 1-42, which is a basic constituent of amyloid plaques, binds with extracellular transmembrane receptor nicotine acetylcholine receptor α7 (nAChRα7) in Alzheimer's disease.

Materials and Methods: In the current study, a computational approach was employed to explore the active binding sites of nAChRα7 through Aβ 1–42 interactions and their involvement in the activation of downstream signalling pathways. Sequential and structural analyses were performed on the extracellular part of nAChRα7 to identify its core active binding site.

Results: Results showed that a conserved residual pattern and well superimposed structures were observed in all nAChRs proteins. Molecular docking servers were used to predict the common interactive residues in nAChRα7 and Aβ1–42 proteins. The docking profile results showed some common interactive residues such as Glu22, Ala42 and Trp171 may consider as the active key player in the activation of downstream signalling pathways. Moreover, the signal communication and receiving efficacy of best-docked complexes was checked through DynOmic online server. Furthermore, the results from molecular dynamic simulation experiment showed the stability of nAChRα7. The generated root mean square deviations and fluctuations (RMSD/F), solvent accessible surface area (SASA) and radius of gyration (Rg) graphs of nAChRα7 also showed its backbone stability and compactness, respectively.

Conclusion: Taken together, our predicted results intimated the structural insight on the molecular interactions of beta amyloid protein involved in the activation of nAChRα7 receptor. In future, a better understanding of nAChRα7 and their interconnected proteins signalling cascade may be consider as target to cure Alzheimer's disease.

ARTICLE HISTORY
Received 11 May 2018
Revised 16 September 2018
Accepted 11 October 2018

KEYWORDS
Alzheimer's disease; computational modelling; molecular docking; dynamic simulation; Aβ42; nAChRα7

Introduction

Amyloid beta (Aβ) is a basic constituent of amyloid plaques, contains 1–42 amino acids, and binds with transmembrane nicotine acetylcholine receptor α7 (nAChRα7) receptor in Alzheimer's disease [1–3]. Aβ42 has more hydrophobic behaviour and the greater propensity to aggregates into fibrils and plaques compared to Aβ40 [4,5]. Prior research showed that the accumulation of Aβ42 results in lysis and selective loss of neurons particularly from entorhinal cortex and hippocampus [6,7].

The nAChRs are ion channel proteins that are particularly distributed in the neuromuscular junction, autonomic ganglia and mostly in the brain [8–10]. It has been studied that Aβ42 particularly interacts with nAChRα7 and upregulates it in the hippocampal cultures [11–13]. Another study also showed that the accumulation of Aβ results in an upregulation of hippocampal nAChRα7 in aged Tg2576 mice [13,14]. Furthermore, the higher concentrations of Aβ42 with longer time results in dysregulation of nAChRα7 and causes interruption of extracellular-signal regulated kinase and cAMP response element-binding protein (ERK1/2-CREB) signaling pathway [15]. This interfering of Aβ42 with nAChRα7 leads to the activation of phosphorylation of signaling proteins (ERK and CREB) which results in memory impairment and causes AD [13,16]. Therefore, physiological concentrations of Aβ42 in hippocampus impinge upon signal

CONTACT Sung-Yum Seo dnalove@kongju.ac.kr Department of Biological Sciences, College of Natural Sciences, Kongju National University, Gongju, Chungnam-do 32588, Republic of Korea

transduction cascades which are important for synaptic plasticity, learning and memory and homeostasis [13].

In the current study, a computational approach was employed to explore the binding interaction of Aβ42 against nAChRα7. The sequences conservation analyses were performed on the selected nAChRs using a multiple sequence alignment (MSA) tool. The three-dimensional (3D) structures of Aβ42 was accessed from PDB whereas, nAChRα7 structure was predicted by homology modelling approach. A detailed structural analysis on both proteins was performed using various computational tools and servers. Protein–protein docking experiment were performed using three online servers to check the residual involvement in the protein interactions and their significance in downstream signaling pathways. Furthermore, a molecular dynamic (MD) simulation experiment was performed to generate the RMSD and RMSF graphs to check the stability of protein backbone in docking experiment. Moreover, SASA and Gyration analysis was done to check the overall protein soluble surface area and compactness of proteins. Our modelling work aims at better understanding of nAChRα7 and their interconnected protein signaling cascades.

Methodology

Repossession of human nAChRs sequences and analysis

Human nAChRs protein sequences were retrieved from the UniProt database (http://www.uniprot.org/) having IDs P02708, Q15822, P32297, P30926, P30532, Q15825, P36544, Q9UGM1 and Q9GZZ6, respectively. The MSA analysis was carried out through Clustal Omega by using standard parameters to observe the conservation pattern in the selected nAChRs (nAChR1–7 and nAChR9–10) amino acids sequences [17]. Moreover, Aliview was employed to visualize the aligned sequences of all nAChRs proteins [18].

Retrieval of human Aβ42 and prediction of extracellular nAChRα7 protein

The crystal structure of Aβ42 fibril was retrieved from Protein Data Bank (PDBID: 2BEG). Since the nAChRα7 is not available in PDB, therefore, online Swiss modeling server was used to predict nAChRα7 structure [19]. In nAChRα7 structure prediction, the human neuronal acetylcholine receptor subunit α4 was used as structural template having PDBID 5KXI which showed 45% sequence identity with target protein (Figure S1). The accessed protein structures were minimized by using UCSF Chimera 1.6 by employing conjugate gradient algorithm and amber force field [20]. Furthermore, the stereo-chemical properties of targeted structures were accessed through Molprobity server [21] and ProSA web [22]. Moreover, their theoretical isoelectric point (*PIs*) extinction coefficients, aliphatic and instability indexes, and Grand Average of Hydropathy (GRAVY) values were predicted by using Protparam tool [23]. The protein structural reliability was confirmed through were Molprobity server by generating Ramachandran plots [24]. The hydrophobicity graphs for both proteins were generated through Discovery Studio 4.1 Client [25]. Finally, VADAR 1.8 server was used to predict the percentage values of α-helices, β-sheets, coils and turns [26].

Protein–protein docking

To obtain the accurate binding results with minimum error prediction, we have employed ClusPro 2.0 [27], HADDOCK [28] and FireDock [29] online protein–protein docking servers to dock the Aβ42 against nAChRα7. A protein–protein docking experiment was performed to acquire the best conformation between Aβ42 and nAChRα7 using ClusPro 2.0 server. ClusPro 2.0 predicts docking results in four different categories of predicted models such as balanced, electrostatic-favored, hydrophobic-favored and VdW + Elec. In the docking results, predicted models were ranked by cluster size [30] and best models were selected from all categories. We discarded the complexes with unacceptable penetrations of receptor atoms to the atoms of the ligand. Finally, remaining candidates were ranked according to the geometric shape and complementarity scores.

Another docking server HADDOCK 2.2 was employed to check the significant conformational pose of Aβ42 against nAChRα7. The active and passive amino acids of selected proteins were predicted through CPROT tool [31]. These predicted active-passive amino acids are used to define a network of ambiguous interaction restraints between the molecules to perform docking [32]. The HADDOCK docking approach is consisted of three stages: (i) the minimization of rigid body energy (it0), (ii) refinement in torsion angle space (it1), and (iii) a final explicit solvent refinement (water). In each docking stage the solutions are ranked on the basis of scoring functions used in HADDOCK protocol. Finally, all the generated docked complexes were ranked and evaluated based on their scoring values.

Another protein–protein docking server FireDock was used to judge the interaction behaviour between

both proteins. In FireDock, fast rigid-body docking algorithm was used to address the protein flexibility and scoring calculations of generated docked complexes. Finally, 100 docking complexes were selected for further analysis. All the generated docked complexes were ranked as per generated score values. The interaction profile between Aβ42 and nAChRα7 among all docking complexes were visualised through Discovery Studio (4.1) (Accelrys Software Inc., San Diego, CA) and UCSF Chimera 1.10.1, tools respectively. LIGPLOT was employed for two dimensional graphical representations of docked complexes [33]. Furthermore, signaling efficacy graphs for all these best docked complexes were generated by DynOmic online portal using elastic network models [34].

Molecular dynamics (MD) simulations

MD simulations were carried out by GROMACS 4.5.4 package [35] with GROMOS 96 force field [36] to understand the protein backbone flexibility. To accomplished MD simulation, we adjusted few parameters. Initially, ions were added to neutralize system charge. Energy minimization was done by the steepest descent approach (1000 ps) for targeted protein structure. Moreover, to better perform energy minimization, we adjusted nsteps =50,000 with energy step size (emstep) 0.01 value. Energy calculations were carried out by particle mesh Ewald (PME) method. Moreover, for electrostatic and van der Waals interactions; cut-off distance for the short-range VdW (rvdw) was set to 14 Å, rlist and nstlist values were fixed as 1.0 and 10, respectively, in em.mdp file [37]. It permits the use of the Ewald summation at a computational cost comparable with that of a simple truncation method of 10 Å or less. For covalent bond constraints the linear constraint solver [38] algorithm was employed with 0.002 ps time step. Finally, MD simulation was performed at 50 ns with nsteps 25,000,000 in md.mdp file. Multiple protein structural analysis such as RMSD/RMSF, SASA and Rg of protein back bone were analysed using Xmgrace software (http://plasma-gate.weizmann.ac.il/Grace/) and UCSF Chimera 1.10.1 software.

Results

Sequences and predicted structures analysis of extracellular domains of nAChRs

The human protein sequences of nAChRs (nAChR1–7, 9–10) and their predicted structures were aligned to observe the residual conversation pattern. The sequential and structural analyses showed that there is a close similarity among all nAChRs sequences which depicted their conservation pattern. The average sequence identity and similarity among all selected proteins isoforms (nAChR1–7, 9–10) were calculated as 40% and 66%, respectively. The sequences of nAChRs results showed that the common residues may have a significant role in downstream signaling pathway. The superimposed structures of extracellular domain of nAChRs showed that there is close homology and similarity pattern among the structural architectures such as loops, beta sheets coils and turns, respectively (Figure 1). The extracellular part of all nAChRs is known as target template for Aβ42 binding and nAChRα7 is most significant target receptor in AD, through the interaction with aggregated Aβ42 [39].

Physio-chemical analysis of Aβ42 and nAChRα7

The physio-chemical properties such as molecular weight and theoretical *pI* of both Aβ42 and nAChRα7 structures were calculated through ProtParam tool. The molecular weight and *pI* values of both Aβ42 and nAChRα7 structures were calculated by the aggregation of average isotopic masses and pK values of linear amino acids sequences. Prior research data is justified the wide range of *pI* values (4.31–11.78) among proteins [40,41]. Our predicted results showed that both Aβ42 and nAChRα7 structures possessed (4.37 and 4.39, respectively) comparable *pI* results with standard values. These predicted values of *pIs* justified the reliability of Aβ42 and nAChRα7 structures. The sum of hydropathy values of all residues present in protein sequence is known as GRAVY value [42]. Prior scientific data showed that positive and negative values of GRAVY show the hydrophobic and hydrophilic behaviour of proteins [40]. Our generate that showed that both Aβ42 and nAChRα7 possessed 1.454 and −0.405 GRAVY values which justified their hydrophobic and hydrophilic behaviour, respectively. Furthermore, the aliphatic index values of Aβ42 and nAChRα7 were computed from the equation as mentioned in supplementary data (Equation i). The predicted physiochemical properties showed the reliability, efficacy and stability of the proteins. Furthermore, ProSA tool depicted the overall quality scores of both proteins on the basis of *z*-score value. Moreover, the predicted structure accuracy is also conducted by VERIFY 3D tool. The VERIFY 3D tool determines the compatibility of an atomic model (3D) with its own amino acid sequence (1D) by assigning a

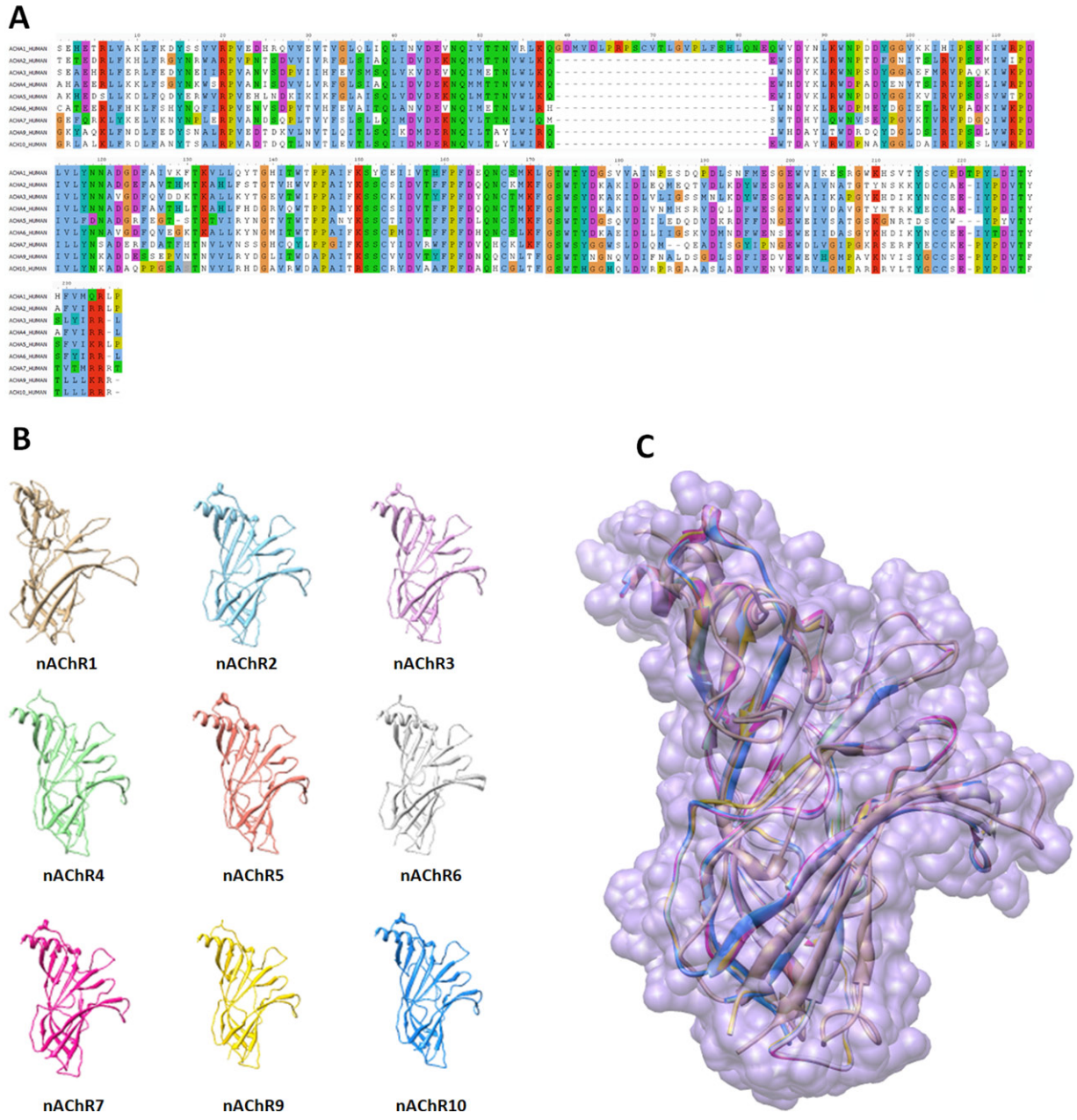

Figure 1. Residual conservation pattern and structural overlapping of nAChRs structures. (A) The alignment of amino acids sequences of human nAChRs (nAChR1–7, 9–10). (B) Three dimensional (3D) predicted structures of nAChRs are shown in different colors. (C) Superimposed predicted structures of nAChRs in surface format.

Table 1. Structural analysis of protein structures.

Structure evaluation parameters	Aβ42	nAChRα7
Theoretic-al *pI*	4.37	5.40
GRAVY	1.454	−0.482
AI	142.31	73.59
II	17.82	44.76
Z-score	−1.3	−5.05

AI = Aliphatic index; GRAVY = Gran average of hydropathicity; II = Instability index.

structural class based on its location and environment (alpha, beta, loop, polar, nonpolar etc) and comparing the results to good structures. The graphical depiction of ProSA graphs of both predicted structures (Aβ42 and nAChRα7) are mentioned in supplementary data (Figures S2, S3). The predicted values of both proteins (Aβ42 and nAChRα7) are mentioned in Table 1.

Structural analysis of predicted Aβ42 and nAChRα7 protein

The Aβ42 and nAChRα7 were evaluated to test their structural architectures on the basis of structural coordinates. The VADAR 1.8 analysis showed that the residual architecture of Aβ42 and nAChRα7 and statistical percentage values of helices, sheets, coils and

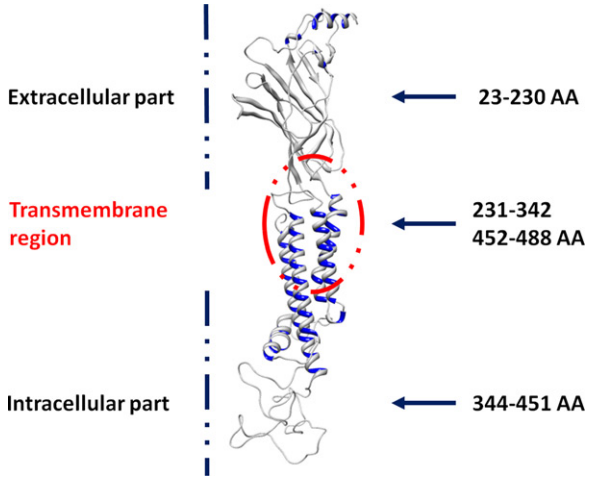

Figure 2. The predicted structure of nAChRα7. The structure is represented in gray color, while interior beta sheets are depicted in blue color. Red circle shows the transmembrane region of target structure.

turns. The Aβ42 only consists of coils, whereas nAChRα7 contain helices 5%, beta sheets 54%, coils 40% and turns 21%, respectively. Furthermore, the Ramachandran graphs and values also confirmed the reliability and efficacy of Aβ42 and nAChRα7 structures. The Ramachandran plots indicate that 98.50% and 98.99% of all residues in Aβ42 and nAChRα7 were present in the favoured regions. The overall protein structure of nAChRα7 is shown in Figure 2. The graphical depiction of Ramachandran and hydrophobicity graphs of Aβ42 and nAChRα7 are shown in supplementary data (Figures S4, S5).

Docking analysis of Aβ42-nAChRα7

The protein–protein docking is important and noteworthy method to explore the functional binding residues involved in downstream signaling pathways [43,44]. In our study, three protein–protein docking servers were employed to predict the functional binding sites and their interacted residues in Aβ42-nAChRα7 docked complexes.

ClusPro 2.0 docking energy calculation in Aβ42-nAChRα7 docked complexes

To evaluate our docking results, the ClusPro 2.0 server was employed to obtain the best conformational position in Aβ42-nAChRα7 docked complexes. The best-docked complexes were ranked as per best cluster size. ClusPro 2.0 generates four sets of models using four different sets of energy coefficients that we call: (1) balanced, (2) electrostatic-favored, (3) hydrophobic-favored and (4) van der Waals electrostatics.

Table 2. Docking energy values for complexes using ClusPro.

Complexes	Cluster size	Representative	Weighted score
1	79	Center	−966.8
		Lowest energy	−1226.9
2	72	Center	−1021.1
		Lowest energy	−1090.3
3	61	Center	−1000.4
		Lowest energy	−1059.0
4	41	Center	−1127.3
		Lowest energy	−1185.3
5	40	Center	−1018.4
		Lowest energy	−1133.2
6	40	Center	−1118.0
		Lowest energy	−1118.0
7	39	Center	−977.7
		Lowest energy	−1096.5
8	37	Center	−1032.5
		Lowest energy	−1082.1
9	36	Center	−974.7
		Lowest energy	−1054.5
10	30	Center	−1038.4
		Lowest energy	−1078.7

Complexes with favorable surface complementarities are retained and scrutinized on the basis of good electrostatic and desolvation free energies. ClusPro also generates cluster centers that are a representative set of complexes that form a cluster. The cluster centers are ranked according to cluster sizes. Our docking server results show that the best-docked complex has cluster size is 79 having centered and lowest energy −966.8 and −1226.9, respectively score values (Table 2).

HADDOCK analysis of Aβ42-nAChRα7 docked complexes

In order to persue the accurate docking results, HADDOCK docking server was used to get the best conformational poses between Aβ42 and nAChRα7 docking complexes. The best-docked complexes were dissected on the basis of HADDOCK scoring values. Generally, the HADDOCK score is relay on different energy values including electrostatic, van der Waals, desolvation and restraints violation energies, respectively [45–47]. In our results, −104.1 was the best score value which showed the best conformational position of Aβ42 against the active region of nAChRα7. The *z*-scores may also be positive or negative, with a positive value indicating the score is above the mean and a negative score indicating it is below the mean. Therefore, lower and negative *z*-score values are significant copared to positive values [28]. The best predicted z-score value is −1.6 for Aβ42-nAChRα7 among all docked complexes. The predicted docking energy and score values are mentioned in Table 3.

Table 3. Docking energy values of docking complexes using HADDOCK.

Complexes	HADDOCK score	Cluster size	RMSD	Electrostatic energy	Buried surface area	*Z*-score
1	−104.1	11	5.4	−113.0	2137.5	−1.6
2	−80.9	5	6.1	−118.7	1540.8	−0.6
3	−77.9	6	7.6	−28.0	1875.7	−0.5
4	−73.4	37	8.6	−169.6	1534.4	−0.3
5	−58.7	82	8.1	−69.0	1384.7	0.3
6	−38.1	9	10.2	−143.8	827.3	1.1
7	−26.3	4	6.6	−26.0	1215.4	1.6

Table 4. Docking energy values of docking complexes using FireDock.

Complexes	Global energy	Attractive Vdw	Repulsive Vdw	ACE	HB
1	−40.98	−35.04	18.13	−4.09	−0.28
2	−38.08	−36.09	23.75	−3.46	−2.86
3	−5.44	−27.15	19.26	−1.31	−2.03
4	−2.16	−6.64	0.84	0.57	0.00
5	0.79	−4.91	1.56	−1.41	−1.71
6	5.37	−6.37	1.02	0.32	−0.35
7	8.99	−1.65	0.20	−0.05	−0.84
8	37.51	−19.76	62.60	0.71	−2.30
9	148.93	−19.88	219.18	−1.10	−2.55
10	5143.22	−66.09	6623.07	−26.79	−13.85

FireDock evaluation of Aβ42-nAChRα7 docking complexes

To re-examine our protein–protein docking results, we further analysed the FireDock docking Aβ42-nAChRα7 complexes on the basis of generated energy values. FireDock docking results, the predicted docked complexes were ranked as per best global energy values (kcal/mol). Furthermore, both the atomic contact energy (ACE) and hydrogen bonds (HB) values of docking complexes were also keenly monitored to select the best-docked complex. The predicted global energy value −40.98 showed the best conformation position of Aβ42 against nAChRα7 as compared to all other docked complexes (Table 4).

Binding interaction pattern between Aβ42 and nAChRα7

The interaction (hydrogen/hydrophobic) pattern among proteins is involved in multiple biological processes and important to understand the underlying molecular mechanisms in different diseases [48]. Prior scientific reports showed that protein stability depends upon the interactions such as HB among amino acids in two ineracting proteins. The most suitable and favorable HB distance is from 1.9 to 2.5 Å, however, another research study also described this distance with this range 1.5–3.8 Å [49–51].

Based on all docking results, a good binding interactions patteren between Aβ42 and nAChRα7 was observed in selected docked complexes. ClusPro 2.0 docking results showed various amino acids of Aβ42 such as Leu34, Glu22, Asp23, Ala42, Asn27, Gly29 and Ala30 forms HB with nAChRα7 residues Trp171, Tyr217, Ser117, Ser177, Arg42, Asp119, Glu41, Leu40 and Asp47. In more detail, Asn27 and Gly38 (Aβ42) form HB with Ser48 and Asp111 having bonds length 2.85 and 3.05 Å, respectively. Leu34 and Val36 also make HB with Arg42 and Tyr173 with very bond lengths 3.12 and 2.64 Å, respectively. Moreover, Gly25, Glu22, Ala21, Gly33 and Ala30 of Aβ42 forms active HB with Trp176, Lys214, Tyr217 and Asp47 with bond distances 2.89, 2.61, 2.78, 2.59 and 2.85 Å, respectively. The binding of these residues ensured the good conformation of Aβ42 with nAChRα7 and stability of the docked complex. The binding interactions inside the active region of Aβ42 with nAChRα7 is mentioned in Figure 3(A).

In HADDOCK results seven HB were detected in Aβ42-nAChRα7 docked complex. The Aβ42 residue Lys28 and Met35 form HB with Asp153 and Asp119 with bond length 2.65 and 2.95Å, respectively. Gly29, Ile31, Val18 and Glu22 also form good hydrogen interactions with Gln70, Trp171 and Arg208, respectively. Both Gly29 and Ile31 form the strong HB with single residue Gln70 having bond length 2.07 and 2.05 Å, respectively. Further, Val18 makes single bond against Trp171 with bond length 2.78 Å. Glu22 shows more interaction behaviour and form the double bond against Arg208 with bond distances 2.62 and 3.31 Å, respectively. Glu22 and Trp171 were common interacted residues of Aβ42 and nAChRα7 in both docking servers (ClusPro and HADDOCK) (Figure 3B). The 2D binding interactions between Aβ42 and nAChRα7 is mentioned in supplementary data Figure S4.

Furthermore, FireDock docked complexes of Aβ42 and nAChRα7 were also analyzed on the basis of interaction pattern (Figure 3C). Hydrophobic interactions were observed between Thr99, Leu131 and Gln139 against Ala42 and Ile41, respectively. ClusPro results show good interactions pattern compared to HADDOCK and FireDock results. The 2D depictions of all docking server results are mentioned in in Figure 4A–C.

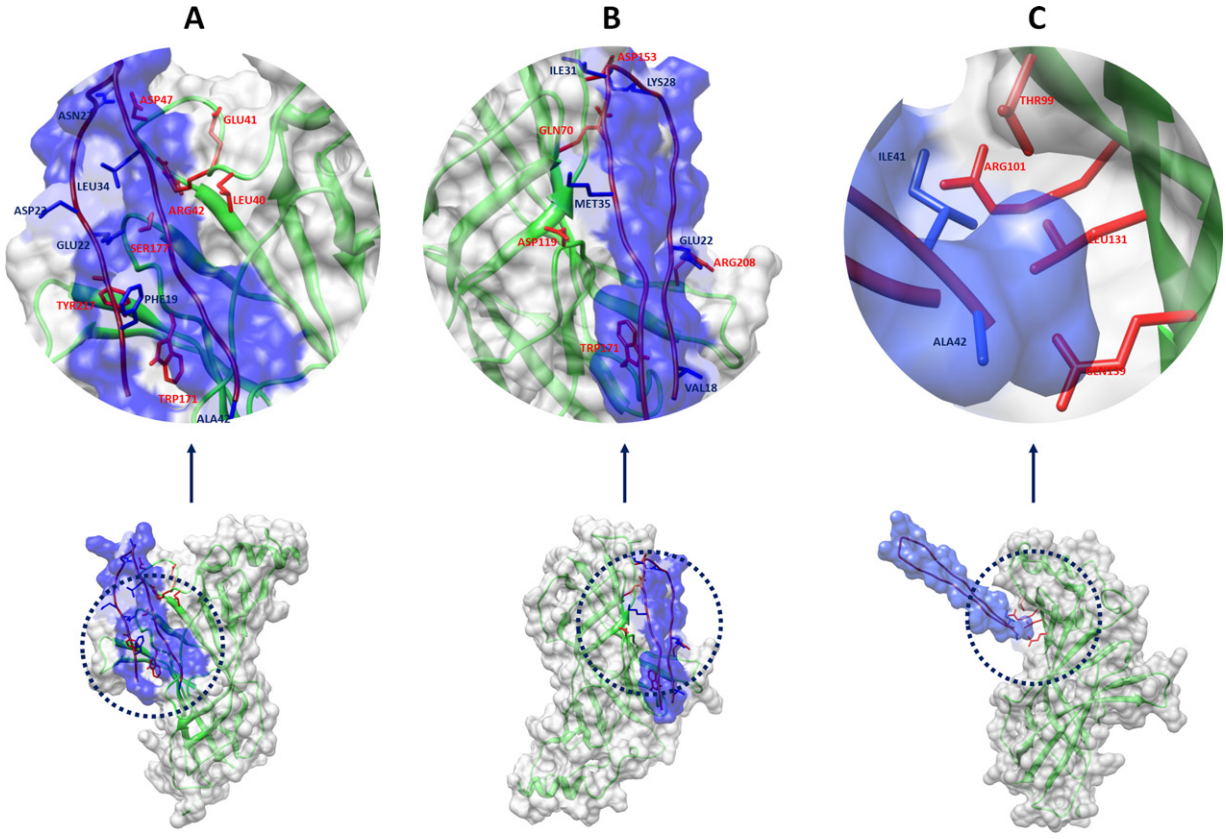

Figure 3. Docking interactions between Aβ42 and nAChRα7. (A) ClusPro docking complex, (B) HADDOCK docking complex and (C) FireDock results. The surface structure of nAChRα7 is shown in purple color, while Aβ is highlighted in gray, brown and yellow colors in ClusPro, HADDOCK and FireDock server, respectively. The red dotted lines represent HB distance in angstrom (Å).

The common interacted residues Glu22, Ala42 and Trp171 may show their active participation in the activation of downstream signaling pathways. The predicted results showed that these residues may consider as the active key player in the activation of downstream signaling pathways. The common interacted docking residues depicted by docking servers are shown in Table 5.

Signal communication and receiving efficacy of docking proteins

The DynOmics addresses the dynamic and allosteric behaviour of biomolecules such as proteins. It also identify the functional sites and analysing signal communication properties of protein structures. DynOmic server was used to predict the signal communication and receiving properties of proteins through residual interactions in best-docked complexes. The hitting time of standard deviation displays the standard deviation vs mean value for both response and perturbation sites. The standard deviation of hitting time displays the standard deviations vs mean value for both response sites and perturbation sites. The standard deviation refers to the variation in the hitting time of both interacted residues. Generally, the residues exhibiting higher average hitting times also depict a higher standard deviation value. In all three docking complexes, the average standard values for interacted residues in communicating site is fluctuated while for receiving site is quite similar in all docking complexes. HADDOCK and FireDock complexes display higher standard deviations values with respect to average signaling rate of communicating sites compared to Cluspro docking complex. However, sites with low average hitting time and standard deviation are distinguished by their efficient and precise function with regard to signal transmission. The standard deviation values for hitting site are range from 50 to 150 in all docking complexes. The Cluspro results showed that Aβ42 residues (black circles) displayed little scattered pattern against nAChRα7 (Figure 5A), while FireDock and HADDOCK results showed Aβ42 residues were accumulated in unique pattern (Figures 5B, C).

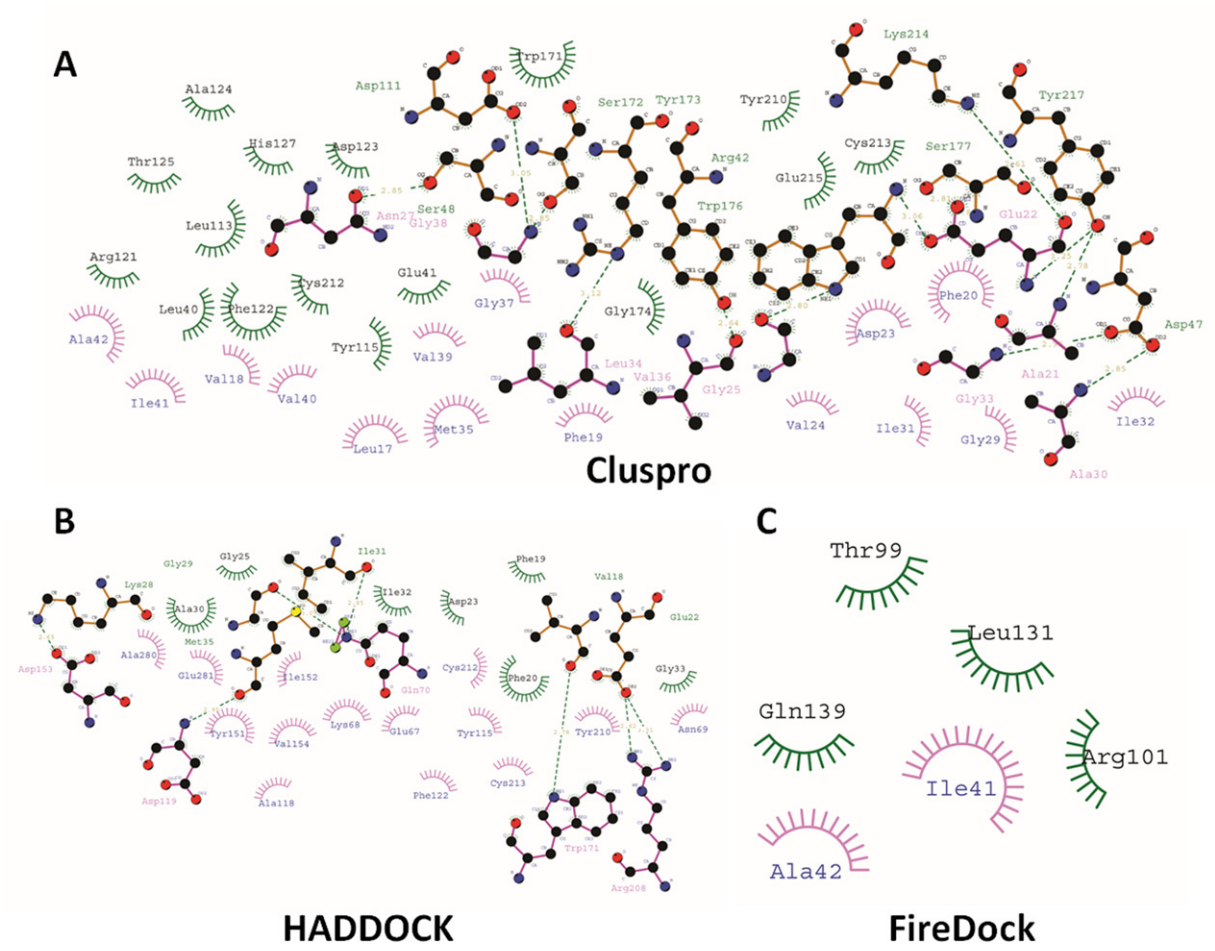

Figure 4. 2D graphical depiction of docking complexes: (A) ClusPro docking complex, (B) HADDOCK docking complex and (C) FireDock results. The green dotted lines represent hydrogen bonding among residues. The Aβ42 and nAChRα7 residues are mentioned by pink and green color respectively.

Molecular dynamic simulation analysis

Root mean square deviation and fluctuation analysis

MD simulation study at 50 ns by using Gromacs 4.5.4 tool was employed to interpret the amino acids flexibility among best-docked structures by generating RMSD and RMSF graphs. Furthermore, SASA (A^2) and Rg analysis were also determined to check the compactness of protein structure. The RMSD results showed that protein backbone deviation and fluctuations with the passage of simulation time frame from 0 to 50 ns.

In ClusPro results, the graph line showed minor fluctuations from 0 to 2500 ps with RMSD value 0.45 nm (Green). While from 2500 to 10,000 ps the graph line remains stable having little fluctuations with average RMSD value 0.3 nm. After that, from 10,000 to 20,000 ps little increasing trend was observed whereas, a sudden increasing trend fluctuations were observed at time 22,000 ps and RMSD value raised up to 0.5 nm. From 22,000 to 30,000 ps the decreasing and increasing trend with little fluctuations was observed while the RMSD value remains same 0.5 nm. From, 30,000 to 50,000 ps graph line remain stable compared to previous time. At time 45,000 ps little increasing trend was observed while after that again downward trend was seen in graph line. The overall results depict the stability of the protein in the simulation time because the average RMSD values remain same with little deviations.

In HADDOCK results, the graph line is highlighted in red color. The overall result showed that the generated graph line was comparatively much fluctuated and showed increasing trend in the starting simulation time frame. From 0 to 5000 ps the graph line shows an increasing trend with RMSD value 0.75 nm. After that, from 5000 to 10,000 ps decreasing and increasing trends were observed in graph line having RMSD approximately 0.5 nm. After that, from 10,000 to 14,000 ps time again increasing trend was observed with higher RMSD value 0.55 nm. From 14,000 to

Table 5. Residual analyses were through HB interactions in docking structures.

		Residues involve in hydrogen/hydrophobic bindings in docking complexes		
Complexes	Target proteins	ClusPro	HADDOCK	FireDock
1	Aβ42	Leu34, Glu22, Asp23, Ala42, Asn27, Gly29, Ala30	Met35, Gly29, Lys28, Ile31, Val18, Glu22	Ile41, Ala42
	nAChRα7	Trp171, Tyr217, Ser117, Ser177, Arg42, Asp119, Glu41, Leu40, Asp47	Asp153, Asp119, Gln70, Trp171, Arg208	Thr99, Leu131, Gln139, Arg101
2	Aβ42	Leu17, Ser26, Lys28, Ala30, Ile31, Gly33, Met35, Val36	Gly33, Ile32, Ala30, Gly29	Glu22
	nAChRα7	Asn38, Leu40, Glu41, Asp47, Tyr86, Glu120, Ser177, Trp171, Tyr217	Gln70, Ser172, Lys68, Ala280	Gln61
3	Aβ42	Phe19, Ala21, Glu22, Asp23, Asn27, Lys28, Gly29, Val136, Val40	Gly38, Val39, Phe19, Leu17	Leu17, Phe19, Val36
	nAChRα7	Asp111, Phe119, Glu120, Arg121, Phe122, Lys147, Trp171, Lys214, Tyr217	Val154, Glu281, Glu67, Asp64, Asp66	Lys68, Asn69,
4	Aβ42	Leu17, Phe19, Glu22, Gly25, Asn27, Lys28, Gly29, Ala30, Gly38, Ala42	Asn27, Met35, Asp23, Ala42	Gly37
	nAChRα7	Lys68, Asn69, Gln70, Tyr151, Ser117, Phe122, Tyr173, Asp111, Arg42, Lys68	Trp171, Lys165, Trp156, Arg155	Asn69,
5	Aβ42	Leu17, Ala21, Gly29, Asn27, Ala30, Asp23, Ala42, Leu34	Lys28, Gly29, Ala30, Gly33	Val36
	nAChRα7	Tyr37, Tyr173, Asn36, Glu41, Trp171, Asn38, Gly105, Tyr115, Lys109, Leu40	Glu67, Lys68, Glu281, Val154	Ile201
6	Aβ42	Lys28, Gly38, Val124, Ile41, Gly29, Ile31, Asp23, Met35, Val39	Phe20, Glu22, Met35, Val39	Ala30, Gly29, Asn27
	nAChRα7	Asp64, Asp66, Ser177, Asp111, Ser172, Lys147, Thr125, Tyr173, Glu120, Phe122, Arg121	Gln70, Tyr151, Arg155	Val199, Arg227
7	Aβ42	Leu34, Phe19, Leu17, Ala21, Val40, Ile41, Gly38, Asp23, Glu22	Asp23	Gly37, Gly33, Val24
	nAChRα7	Glu120, Asp111, Trp171, Tyr173, Tyr115, Asp119, Arg121, Phe122	Tyr151	Asp119, Lys68, Tyr151
8	Aβ42	Asn27, Gly38, Leu34, Val36, Gly25, Gly33, Ala21, Ala30, Glu22	Gly33, Val40, Ile32, Ala30, Gly29	Ile31, Gly37, Val39
	nAChRα7	Asp111, Ser48, Ser172, Tyr173, Arg42, Trp176, Ser177, Lys214, Tyr217, Asp47	Gln70, Lys68, Ser172, Ala280	Asn193, Asp66, Asn69

20,000 ps time frame the graph trend line shows a decreasing and increasing pattern, respectively; however, their RMSD value remains the same. From 20,000 to 30,000 ps time a little stable with increasing trend in graph line was observed with little fluctuations. After that, from 30,000 to 50,000 ps stable pattern was observed with very little fluctuations and surprisingly the RMSD value also remains same in this time period. Both ClusPro and HADDOCK graphs line remained stable after 30,000 ps time with little fluctuations.

FireDock results graph line (purple color) is a stable throughout the simulation time frame. Initially, the graph line shows an increasing trend from 0 to 2500 ps, while after that little decreasing trend was observed and remains stable up to 12,000 ps. From 12,000 to 25,000 ps the graph line remains stable with little fluctuations with the average value of RMSD 0.35 nm. After that little increasing trend was observed up to 30,000 ps and from 30,000 to 50,000 ps the graphs line remains stable which depicts good stability of protein. The comparative analyses justified that ClusPro showed good stable results compared to HADDOCK and FireDock results during the simulation time period. A correlated result were observed in both docking servers (ClusPro and FireDock) and also similar pattern was in simulation results (Figure 6A). The RMSF results of all three docking protein structures dynamically fluctuated from residues N to C terminals (2 to 215 AA). Three fluctuation peaks higher than 0.8 nm appeared in the graph. Residues around 110 and 210 positions showed higher fluctuations in loop regions. The comparative results justify that HADDOCK loop regions showed higher fluctuations compared to ClusPro and FireDock (Figure 6B).

Radius of gyration and solvent accessible surface area analyses

In protein structures, the structural compactness was calculated by the Rg graph. It has been observed that the firmly folded proteins show steady value of Rg, whereas the misfold/unfold regions of proteins depicts highly fluctuated Rg value in MD simulation time. The generated results depicted that the Rg value of all the

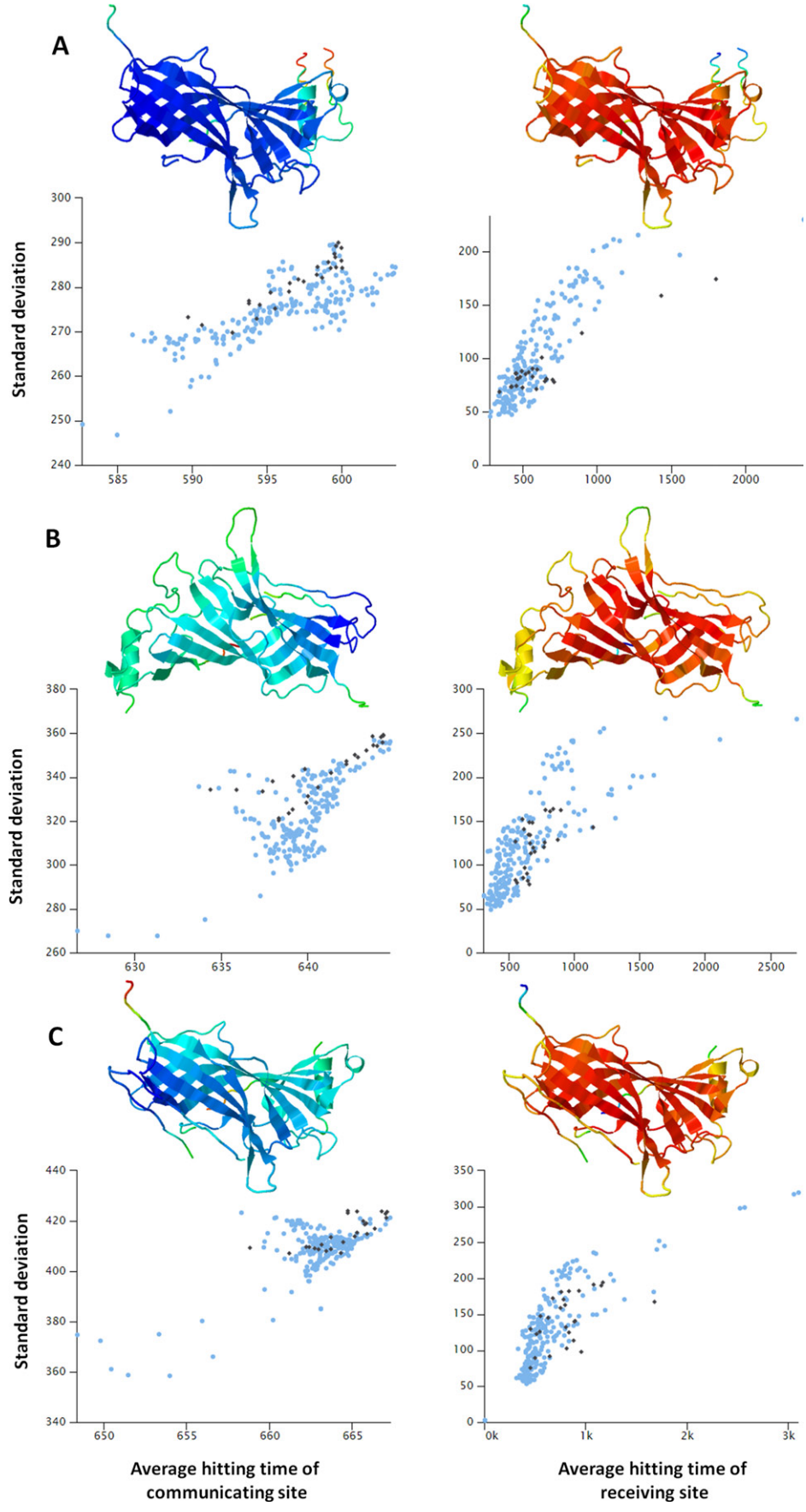

Figure 5. Communicating and efficacy sites for all three docking complexes. (A) Cluspro (B) HAADDOCK (C) FireDock. The black dot represents Aβ42 while blue for nAChRα7.

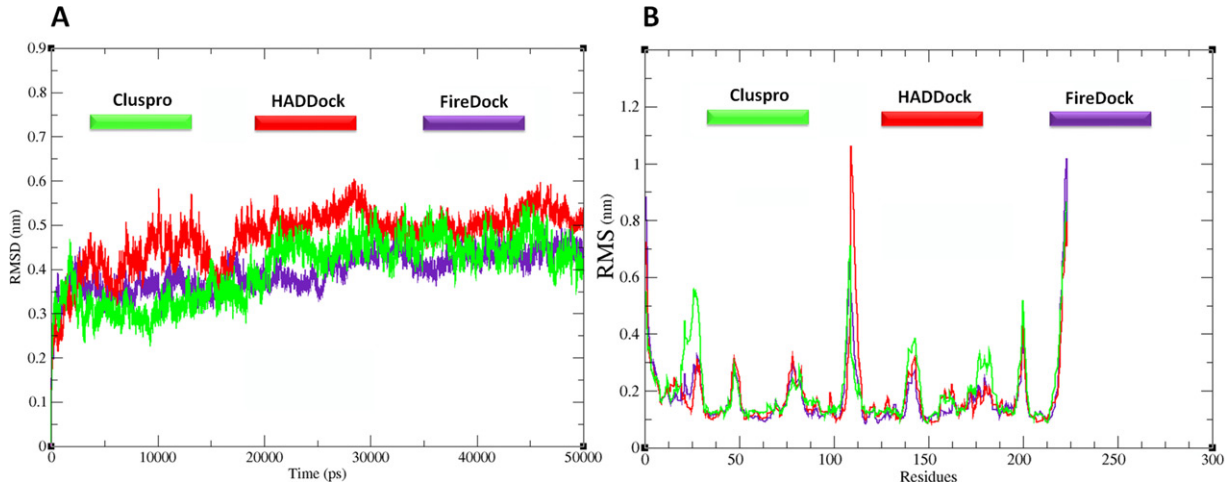

Figure 6. RMSD graph of all the docking structures from 0 to 50,000 ps simulation time frame. (B) RMSF graphs fluctuations of backbone residues in simulation time. Green, red and purple colors represent the ClusPro, HADDOCK and FireDock docking complexes.

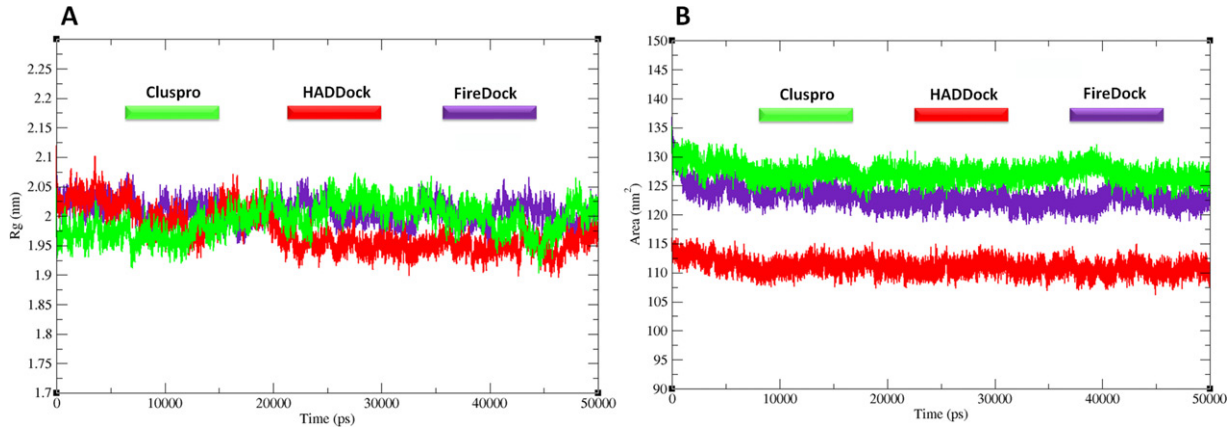

Figure 7. Rg graph of all the docking structures from 0 to 50,000 ps simulation time frame. (B) SASA graph of protein backbone residues in simulation time 0–50,000 ps. Green, red and purple colors represent the ClusPro, HADDOCK and FireDock docking complexes.

docked proteins showed little variation from 1.95 to 2.05 nm. A stable behaviour was observed from 0 to 10,000 ps, whereas from 10,000 to 2000 ps time little fluctuation was observed. Later on, in whole simulation time, no higher fluctuations were observed in graphs lines and Rg value remains stable at 2 nm. The comparative results showed that FireDock and ClusPro (purple and green) structures depict more stability as compared to HADDOCK graph line (red). The fluctuations in Rg value of docking structure of (HADDOCK) showed its unstable behaviour in the binding complex which may results in disturbance of active binding region nAChRα7, leading to the conclusion that disturbance in receptor may disturb the downstream signaling pathways (Figure 7A).

The SASA results showed that the values of ClusPro and FireDock complexes are centered on 127 nm^2 in the simulations graphs while HADDOCK graph line was centered at 112 nm throughout the simulation time 0–50,000 ps. Our MD analyses showed that conformational positions in both ClusPro and FireDock docking servers were remained stable compared to HADDOCK results (Figure 7B).

The mechanistic pathway of nAChRα7 in memory loss

The nAChRs are ion channels proteins widely distributed in the neuromuscular junction, autonomic ganglia and mostly in the brain [8–10]. The aggregated Aβ42 binds with transmembrane receptor nAChRα7 and activates mitogen-activated protein kinase and extracellular-signal regulated kinase (MAPK/ERK) proteins. Both MAPK/ERK signalling proteins undergo phosphorylation and disturb the memory through binding with CREB [13,16,52,53] (Figure 8). Another,

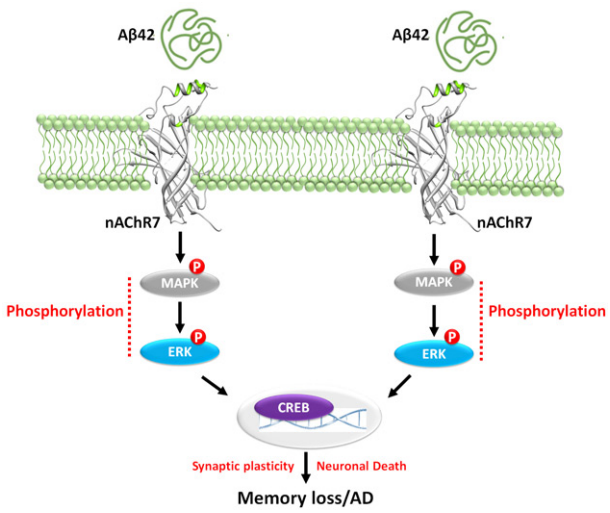

Figure 8. Possible mechanistic pathway of nAChRα7 leading to AD. Gray color nAChRα7 receptor molecule is embedded in bipolar membrane. The aggregated Aβ42 interacts with nAChRα7 and activates MAPK/ERK signaling cascade. Phosphorylation of these signaling proteins enhanced the CREB transcription factor which results in memory loss in hippocampus.

prior research also revealed that the Aβ-peptide alters the hippocampal-dependent synaptic plasticity, memory and mediates synapse loss through the CREB signaling pathway. Moreover, CREB signaling is essential for long-lasting changes in synaptic plasticity that mediates the conversion of short-term memory to long-term memory [54].

Discussion

We have implemented molecular docking and MD simulation techniques to understand the mechanistic insights of Aβ42 interactions against extracellular domain nAChRα7. The sequential (MSA) results depicted that all the extracellular domains of acetylcholine receptors showed a unique similarity and conserved sequence pattern which increases their significance as a target structure to cure AD. The overlapped structural results also showed the close similarity in all nAChRs structures which showed their core conservation pattern and its significance in humans. Based on both sequence and structural results it can be predicted that nAChRα7 could be used as novel target to AD. However, literature data also depicted as nAChRα7 has strong interaction with Aβ42 [39], therefore, by exploring the common interacting residues in both interacted proteins, it could be helpful to better understand the target protein (nAChRα7) and to design some new drug which may work in the treatment of AD.

The protein–protein docking is the most significant approach to explore the functional binding sites and interacted residues among target structures [43,44,55]. The HB play an important role in strengthening the docked complex. The prior research data showed suitable HB distances from 1.9 to 2.5 Å and 1.5 to 3.8 Å, respectively [49–51]. In our docking results the binding interaction patterent and bond lengths were quite comparable with the standard values. The common interacted residues Glu22, Ala42, Trp171, Ser129 and Val132 were observed in all docking results may considered as the active key player in the activation of downstream signalling pathways. The signal communication and efficacy of docking results showed that, in Cluspro results the Aβ42 residues (black circles) displayed little scattered pattern against nAChRα7, while FireDock and HADDOCK results showed Aβ42 residues were accumulated in unique pattern.

MD simulation results showed the stability of protein structures by generating RMSD, RMSF, Gyration and SASA graphs. The comparative analyses of MD simulation results justified that ClusPro docking complex showed good stable results compared to HADDOCK and FireDock results in simulation time period. Moreover, RMSF results of all three docking protein structures dynamically fluctuated from residues N to C terminals (2 to 215 AA). Three fluctuation peaks higher than 0.8 nm appeared in the graph. Residues around 110 and 210 positions showed higher fluctuations in loop regions. The comparative results justify that HADDOCK loop regions showed higher fluctuations compared to ClusPro and FireDock. Furthermore, gyration and SASA results also show the significance of protein stability in binding interaction. Our MD analyses showed that conformational positions in both ClusPro and FireDock docking servers were remained stable compared to HADDOCK results. Our computational analysis showed the binding pattern of aggregated Aβ42 against nAChRα7 and their involvement in AD. Moreover, nAChRα7 could be used as novel target to design novel pharmaceutical agents against AD.

Conclusions

Proteins interact with counter partners and perform functions through the cascade of signaling pathways [56]. The MSA results depicted that extracellular domain of nAChRα7 showed a conserved sequence pattern among other (nAChRs) which increases their significance as a target structures in the betterment of human disease. Docking results justified that the

extracellular part of nAChRα7 and Aβ42 has similar interaction pattern in all three docking servers. Docking results also highlight three common residues (Glu22, Ala42 and Trp171) in both proteins (nAChRα7 and Aβ42) which can be consider as the key player in the activation of downstream signaling pathways. The RMSD, RMSF, SASA and Rg generated graphs showed the good stable behaviour of target proteins. Based upon aforementioned data, our *in silico* analysis depicted that nAChRα7 could be used as novel target to design some novel chemical scaffolds against AD.

Future perspectives

In future, the aforementioned results may open a new gateway for the designing of some novel chemical inhibitors by taking nAChRα7 as a target protein. Recently, most of medicinal chemists and pharmaceutical industries are synthesizing medicinal scaffolds for AD by targeting cholinesterase (acetyl and butyrylcholinesterase). However, our research may help him to design some new chemical inhibitors for the treatment of AD by taking nAChRα7 as a new therapeutic target molecule.

Author's contributions

MH conceived the study under the guidelines of SYS and AAM. HR, LH and SS collected data and performed the experimental work. MH wrote the initial draft of manuscript. HA and NZ make corrections in initial draft. SYS and AAM edited the manuscript and compiled into final format.

Disclosure statement

No potential conflict of interest was reported by the authors.

Funding

This was supported by Basic Science Research Program through the National Research Foundation of Korea (NRF) funded by the Ministry of Education (2017R1D1A1B03034948).

References

[1] Nagele RG, D'andrea MR, Anderson WJ, et al. Intracellular accumulation of β-amyloid 1-42 in neurons is facilitated by the α7 nicotinic acetylcholine receptor in Alzheimer's disease. Neuroscience 2002; 110:199–211.

[2] Wang HY, Lee DH, Davis CB, et al. Amyloid peptide Aβ1-42 binds selectively and with picomolar affinity to α7 nicotinic acetylcholine receptors. J Neurochem. 2002;75:1155–1161.

[3] Wilson CA, Doms RW, Lee VM. Intracellular APP processing and A beta production in Alzheimer disease. J Neuropathol Exp Neurol. 1999;58:787–794.

[4] Iljina M, Garcia GA, Dear AJ, et al. Quantitative analysis of co-oligomer formation by amyloid-beta peptide isoforms. Sci Rep. 2016;6:28658.

[5] Meisl G, Yang X, Hellstrand E, et al. Differences in nucleation behavior underlie the contrasting aggregation kinetics of the Aβ40 and Aβ42 peptides. Proc Natl Acad Sci USA 2014;111:9384–9389.

[6] D'andrea MR, Nagele RG, Wang HY, et al. Evidence that neurones accumulating amyloid can undergo lysis to form amyloid plaques in Alzheimer's disease. Histopathology 2001;38:120–134.

[7] Takahashi RH, Capetillo-Zarate E, Lin MT, et al. Accumulation of intraneuronal β-amyloid 42 peptides is associated with early changes in microtubule-associated protein 2 in neurites and synapses. PLoS One 2013;8:e51965.

[8] Nordberg AGNE. Neuroreceptor changes in Alzheimer disease. Cerebrovasc Brain Metab Rev. 1992;4: 303–328.

[9] Breese CR, Adams C, Logel J, et al. Comparison of the regional expression of nicotinic acetylcholine receptor α7 mRNA and [125I]-α-bungarotoxin binding in human postmortem brain. J Comp Neurol. 1997;387: 385–398.

[10] Hellström-Lindahl E, Mousavi M, Zhang X, et al. Regional distribution of nicotinic receptor subunit mRNAs in human brain: comparison between Alzheimer and normal brain. Brain Res Mol Brain Res. 1999;66:94–103.

[11] Paterson D, Nordberg A. Neuronal nicotinic receptors in the human brain. Prog Neurobiol. 2000;61:75–111.

[12] Wang HY, Lee DH, D'Andrea MR, et al. β-Amyloid1-42 binds to α7 nicotinic acetylcholine receptor with high affinity implications for Alzheimer's disease pathology. J Biol Chem. 2000;275:5626–5632.

[13] Tozaki H, Matsumoto A, Kanno T, et al. The inhibitory and facilitatory actions of amyloid-beta peptides on nicotinic ACh receptors and AMPA receptors. Biochem Biophys Res Commun. 2002;294:42–45.

[14] Dineley KT, Xia X, Bui D, et al. Accelerated plaque accumulation, associative learning deficits, and up-regulation of alpha 7 nicotinic receptor protein in transgenic mice co-expressing mutant human presenilin 1 and amyloid precursor proteins. J Biol Chem. 2002;277:22768–22780.

[15] Bitner RS, Bunnelle WH, Anderson DJ, et al. Broad-spectrum efficacy across cognitive domains by α7 nicotinic acetylcholine receptor agonism correlates with activation of ERK1/2 and CREB phosphorylation pathways. J Neurosci. 2007;27:10578–10587.

[16] Adams JP, Sweatt JD. Molecular psychology: roles for the ERK MAP kinase cascade in memory. Annu Rev Pharmacol Toxicol. 2002;42:135–163.

[17] Sievers F, Higgins DG. Clustal Omega, accurate alignment of very large numbers of sequences. Methods Mol Biol. 2014;1079:105–116.
[18] Larsson A. AliView: a fast and lightweight alignment viewer and editor for large datasets. Bioinformatics 2014;30:3276–3278.
[19] Arnold K, Bordoli L, Kopp J, et al. The SWISS-MODEL workspace: a web-based environment for protein structure homology modelling. Bioinformatics 2006; 22:195–201.
[20] Pettersen EF, Goddard TD, Huang CC, et al. UCSF Chimera-a visualization system for exploratory research and analysis. J Comput Chem. 2004;25: 1605–1612.
[21] Chen VB, Arendall WB, Headd JJ, et al. MolProbity: all-atom structure validation for macromolecular crystallography. Acta Crystallogr D Biol Crystallogr. 2010;66: 12–21.
[22] Wiederstein M, Sippl MJ. ProSA-web: interactive web service for the recognition of errors in three-dimensional structures of proteins. Nucleic Acids Res. 2007; 35:W407–W410.
[23] Gasteiger E, Hoogland C, Gattiker A, et al. The proteomics protocols handbook. Totowa, NJ: Humana Press; 2005;571–607.
[24] Lovell SC, Davis IW, Arendall WB, et al. Structure validation by Calpha geometry: phi,psi and Cbeta deviation. Proteins 2003;50:437–450.
[25] Studio D. (2008). Discovery "version 2.1." San Diego, CA: Accelrys.
[26] Willard L, Ranjan A, Zhang H, et al. VADAR: a web server for quantitative evaluation of protein structure quality. Nucleic Acids Res. 2003;31:3316–3319.
[27] Kozakov D, Hall DR, Xia B, et al. The ClusPro web server for protein-protein docking. Nat Protoc. 2017;12: 255–278.
[28] Van Zundert GCP, Rodrigues JPGLM, Trellet M, et al. The HADDOCK2.2 Web Server: user-friendly integrative modeling of biomolecular complexes. J Mol Biol. 2016;428:720–725.
[29] Mashiach E, Schneidman-Duhovny D, Andrusier N, et al. FireDock: a web server for fast interaction refinement in molecular docking. Nucleic Acids Res. 2008;36:W229–W232.
[30] Comeau SR, Gatchell DW, Vajda S, et al. ClusPro: an automated docking and discrimination method for the prediction of protein complexes. Bioinformatics 2004;20:45–50.
[31] de Vries SJ, Bonvin AM. CPORT: a consensus interface predictor and its performance in prediction-driven docking with HADDOCK. PloS One 2011;6:e17695.
[32] Karaca E, Melquiond AS, de Vries SJ, et al. Building macromolecular assemblies by information-driven docking introducing the haddock multibody docking server. Mol Cell Proteomics 2010;9:1784–1794.
[33] Wallace AC, Laskowski RA, Thornton JM. LIGPLOT: a program to generate schematic diagrams of protein-ligand interactions. Protein Eng Des Sel. 1995;8: 127–134.
[34] Li H, Chang YY, Lee JY, et al. DynOmics: dynamics of structural proteome and beyond. Nucleic Acids Res. 2017;45:374–380.
[35] Pronk S, Páll S, Schulz R, et al. GROMACS 4.5: a high-throughput and highly parallel open source molecular simulation toolkit. Bioinformatics 2013;29:845–854.
[36] Chiu SW, Pandit SA, Scott HL, et al. An improved united atom force field for simulation of mixed lipid bilayers. J Phys Chem B. 2009;113:2748–2763.
[37] Wang H, Dommert F, Holm C. Optimizing working parameters of the smooth particle mesh Ewald algorithm in terms of accuracy and efficiency. J Chem Phys. 2010;133:034117.
[38] Amiri S, Sansom MS, Biggin PC. Molecular dynamics studies of AChBP with nicotine and carbamylcholine: the role of water in the binding pocket. Protein Eng Des Sel. 2007;20:353–359.
[39] Shen JX, Yakel JL. Functional α7 nicotinic ACh receptors on astrocytes in rat hippocampal CA1 slices. J Mol Neurosci. 2012;48:14–21.
[40] Bjellqvist B, Hughes GJ, Pasquali C, et al. The focusing positions of polypeptides in immobilized pH gradients can be predicted from their amino acid sequences. Electrophoresis 1993;14:1023–1031.
[41] Xiong X, Huang S, Zhang H, et al. Enrichment and proteomic analysis of plasma membrane from rat dorsal root ganglions. Proteome Sci. 2009;7:41.
[42] Kyte J, Doolittle RF. A simple method for displaying the hydropathic character of a protein. J Mol Biol. 1982;157:105–132.
[43] Aamir M, Singh VK, Meena M, et al. Structural and functional insights into WRKY3 and WRKY4 transcription factors to unravel the WRKY–DNA (W-Box) complex interaction in tomato (*Solanum lycopersicum* L.). A computational approach. Front Plant Sci. 2017;8: 819.
[44] Westermarck J, Ivaska J, Corthals GL. Identification of protein interactions involved in cellular signaling. Mol Cell Proteomics 2013;12:1752–1763.
[45] McDonald IK, Thornton JM. Satisfying hydrogen bonding potential in proteins. J Mol Biol. 1994;238: 777–793.
[46] Halperin I, Ma B, Wolfson H, et al. Principles of docking: an overview of search algorithms and a guide to scoring functions. Proteins 2002;47:409–443.
[47] Janin J, Henrick K, Moult J, et al. CAPRI: a critical assessment of predicted interactions. Proteins 2003; 52:2–9.
[48] Li Y, Liu Z, Han L, et al. Mining the characteristic interaction patterns on protein–protein binding interfaces. J Chem Inf Model. 2013;53:2437–2447.
[49] Pace CN, Fu H, Fryar K, et al. Contribution of hydrogen bonds to protein stability. Protein Sci. 2014;23: 652–661.
[50] Hubbard RE, Kamran Haider M. Hydrogen bonds in proteins: role and strength. In: Encyclopedia of Life Sciences (ELS). Chichester: John Wiley & Sons, Ltd; 2010; doi: 10.1002/9780470015902.a0003011.pub2.
[51] Buck M, Karplus M. Hydrogen bond energetics: a simulation and statistical analysis of N-methyl acetamide (NMA), water, and human lysozyme. J Phys Chem B. 2001;105:11000–11015.
[52] Davis RJ. The mitogen-activated protein kinase signal transduction pathway. J Biol Chem. 1993;268: 14553–14553.

[53] Graves JD, Campbell JS, Krebs EG. Protein serine/threonine kinases of the MAPK cascade. Ann N Y Acad Sci. 1995;766:320–343.
[54] Saura CA, Valero J. The role of CREB signaling in Alzheimer's disease and other cognitive disorders. Rev Neurosci. 2011; 22:153–169.
[55] Hassan M, Shahzadi S, Alashwal H, et al. Exploring the mechanistic insights of Cas scaffolding protein family member 4 with protein tyrosine kinase 2 in Alzheimer's disease by evaluating protein interactions through molecular docking and dynamic simulations. Neurol Sci. 2018; 39:1361–1374.
[56] Gonzalez MW, Kann MG. Chapter 4: protein interactions and disease. PLoS Comput Biol. 2012;8: e1002819.